Developments in the Built Environment 25 (2026) 100860

Contents lists available at ScienceDirect

Developments in the Built Environment

journal homepage: www.sciencedirect.com/journal/developments-in-the-built-environment

Optimisation of hydraulic lime mortars incorporating an oil-refinery catalyst by-product for sustainable building rehabilitation

Carla Costa [a,*], Sandra Nunes [b,*]

[a] Lisbon School of Engineering (ISEL), Polytechnic University of Lisbon, Rua Conselheiro Emídio Navarro, 1, Lisbon, 1959-007, Portugal
[b] Faculty of Civil Engineering and Geosciences, Delft University of Technology, Stevinweg 1, Delft, 2628 CN, Netherlands

ARTICLE INFO

Keywords:
Spent fluid catalytic cracking catalyst (ECat)
Hydraulic lime-based mortars
By-product upcycling
Historic building rehabilitation
Sustainable construction material
Design of experiments
Multi-objective optimisation

ABSTRACT

This investigation employs a Central Composite Design-based Design of Experiments (DoE) methodology to develop hydraulic lime mortars incorporating equilibrium catalyst (ECat), a by-product generated at the fluid catalytic cracking unit in oil refineries. The derived mathematical models describe the quantitative effects of key mixing variables, specifically ECat content, water-to-binder ratio and water repellent dosage, as well as their cross-interactions, on mortar properties, namely workability, compressive strength, ultrasound propagation velocity and dynamic modulus of elasticity. Numerical optimisation techniques enabled the identification of optimal lime mortar compositions that maximise eco-efficiency while ensuring compliance with both regulatory and technological requirements for diverse masonry applications, including the rehabilitation of ancient buildings. Results confirm the by-product upcyclability of ECat, with feasible incorporation levels up to 56.6 % by mass, yielding mortars with significant potential for reducing the environmental impact of the built environment while advancing the circular economy and fostering technological innovation in the construction sector.

List of abbreviations

AI	(Pozzolanic) Activity Index	PSD	Particle size distribution
AV	Actual variable value	*Rc*	Compressive strength at 91 age days (MPa)
BSE	Backscattering Electron Mode	RSM	Response surface methodology
CAGR	Compound Annual Growth Rate	SandC	Coarser sand
C-A-S-H	Calcium aluminosilicate hydrates	SandF	Finer sand
CCD	Central Composite Design	SEM	Scanning Electron Microscopy
CI	Confidence interval	SSA	Specific surface area
CV	Coded value level	Std. Dev.	Standard deviation
DFlow	Spread flow diameter (mm)	UPV	Ultrasound pulse velocity (km/s)
DOE	Design of Experiments	TI	Tolerance interval (TI)
ECat	Equilibrium Catalyst	XRF	X-ray fluorescence spectrometry
E_d	Dynamic modulus of elasticity (MPa)	w	Water
HL 5	Hydraulic lime of class 5 (EN 459-1)	WA_{24}	24 h water absorption
LF	Limestone filler	WR	Water-repellent
LOI	Loss on Ignition	XRF	X-ray fluorescence spectrometry
Pop	Population		

1. Introduction

Building renovation and rehabilitation, especially of built heritage, have multidimensional impacts (social, environmental, economic, and cultural), including on sustainable development. Aerial and hydraulic lime mortars are particularly convenient to apply in rehabilitation works of historic buildings because their properties are more compatible with old materials, thus preserving their historical value and authenticity (Kang et al., 2019; Zhao et al., 2024; Loke et al., 2024). Aerial lime mortars harden exclusively through the slow reaction of calcium hydroxide with atmospheric carbon dioxide (carbonation), resulting in relatively slow strength development. These mortars are often

* Corresponding authors.
E-mail addresses: carla.costa@isel.pt (C. Costa), s.c.barbosanunes@tudelft.nl (S. Nunes).

https://doi.org/10.1016/j.dibe.2026.100860
Received 12 October 2025; Received in revised form 9 December 2025; Accepted 19 January 2026
Available online 22 January 2026

compatible with historic masonry, mainly due to their high vapour permeability, which reduces moisture entrapment (Mosquera et al., 2006). In contrast, hydraulic lime mortars harden through faster hydration reactions, forming calcium silicate and aluminate hydrates, which provide early strength, followed by slower carbonation that contributes to long-term durability. Thus, hydraulic lime mortars are often preferred in rehabilitation contexts for their balance of faster setting and higher early strength, while maintaining adequate physical and mechanical compatibility with masonry substrates (Segura et al., 2020; Marques et al., 2006; Maravelaki-Kalaitzaki et al., 2005).

The global lime mortar sector is projected to expand at a 3.7 % CAGR by 2031, underscoring the growing emphasis on sustainable construction and the pressing need for heritage preservation (Verified Market Research, 2024b). However, lime production is a non-renewable material-intensive and energy-intensive process, mainly due to the required high-temperature calcination of limestone, which also releases significant carbon dioxide emissions (European Lime Association, 2023; Mineral Products Association, 2023a; Shan et al., 2016a). Since the calcination temperature of hydraulic lime production is higher than that of aerial lime, the former process has a higher environmental impact in terms of energy use and emissions (Bošković and Radivojević, 2024). Therefore, reducing environmental impact of hydraulic limes is crucial (European Lime Association, 2023; Mineral Products Association, 2023a; Shan et al., 2016a), addressing factors such as climate change, natural resource depletion, ecosystem degradation and environmental damage.

Strategies such as partially replacing hydraulic lime with pozzolans reduce embodied CO_2 and energy demand (Grist et al., 2015) and have revealed significant potential to enhance their technological properties, particularly for building rehabilitation. In hydraulic lime mortars, which are the focus of the present study, pozzolans such as metakaolin, zeolite, silica fume, and rice husk ash react with calcium hydroxide, forming additional calcium silicate hydrates (C-S-H) and calcium aluminosilicate hydrates (C-A-S-H), which refine the pore structure, and lead to a denser and less interconnected microstructure that typically increases strength and reduces permeability, thus enhancing durability (Aškrabić et al., 2021; Malathy et al., 2022; Alvarez et al., 2021; Wang et al., 2024; Malathy et al., 2023a). For instance, at specific replacement levels, hydraulic lime mortars with metakaolin additions can reach compressive strengths almost double those of plain hydraulic lime mortars (up to 98 % higher), and similarly significant strength gains have been reported to blended silica-fume hydraulic lime mortars (Malathy et al., 2022; Wang et al., 2024). However, pozzolan incorporation in hydraulic lime-based mortars, particularly beyond optimal content levels, may otherwise reduce compressive strength attributed to either the dilution effect, where the overall binder content is insufficient to maintain the desired mechanical properties or due to the competition between lime hydration and carbonation reactions consuming available portlandite and thus limiting the occurrence of the pozzolanic reaction (Malathy et al., 2023a; Bakolas and Aggelakopoulou, 2019; Cizer et al., 2010). These findings emphasise the importance of carefully optimising the lime replacement ratios. Proper curing strategies, such as high humidity or controlled carbonation, further refine the properties of pozzolan-lime mortars by enhancing their durability and compatibility with historic masonry (Malathy et al., 2022; Cachim et al., 2010). Achieving compatibility with substrates requires balancing several properties, making tailored formulations and curing strategies crucial for specific rehabilitation contexts (Malathy et al., 2022; Malathy et al., 2023b; Loureiro et al., 2020).

Moreover, when the partial lime surrogate is a pozzolanic by-product, industrial symbiosis occurs, benefiting both the by-product supplier by repurposing it and the construction materials sector. Integrating eco-material innovations into mainstream construction enhances the sector's competitiveness, reduces environmental impact, and contributes to EU sustainability goals by reducing waste stockpiles, advancing the Circular Economy and supporting key policies (Waste Framework Directive (European Parliament and Council, 2008) and Circular Economy Action Plan (European Commission, 2020)). It also aligns with the United Nations' 2030 Sustainable Development Goals, namely SDGs #9 (emphasising circular industrial innovation), #11 (promoting heritage-compatible materials), #12 (including waste valorisation), and #13 (targeting CO_2 mitigation) (United Nations, 2015).

Within this scope, this investigation aimed to assess the feasibility of reusing the equilibrium catalyst by-product (ECat), generated at Sines oil refinery (Portugal), as a partial replacement of hydraulic lime in a large-scale industrial mortar formulation for building rehabilitation.

Most oil refineries are equipped with a Fluid Catalytic Cracking (FCC) unit that converts heavy oil into lighter fractions, increasing the yield of higher-value products, such as gasoline (Sadeghbeigi , 2012; Vogt and Weckhuysen, 2015; Oloruntoba et al., 2022). Over time, the catalyst used in this unit gradually loses its required activity, leading to the global annual production of approximately 840 000 tonnes of ECat (Ferella et al., 2019). Typically disposed of in landfills (Leone et al., 2018), ECat appears as a white-grey fine powder (around 75 μm particle size), comprising a faujasite-type zeolite, an amorphous alumina matrix, clay (usually kaolin), a binder (Sadeghbeigi , 2012; Vogt and Weckhuysen, 2015), and contains trace metals, particularly iron, vanadium, and nickel, that accumulate during catalytic operation (Ferella et al., 2016). Leaching studies on ECat report that metal release remains below regulatory limits for classification as non-hazardous in Europe, Taiwan, and the USA (Rattanasak et al., 2001; Antiohos et al., 2006; Su et al., 2000; Fu et al., 2021), while in China is classified as hazardous under local criteria (Fu et al., 2021; Zhang et al., 2021). In Portugal, in 2019, the ECat was reclassified from waste to subproduct for use in mortars production (Agência Portuguesa do Ambiente, 2019). Despite variations in the exact composition - which depend on the fresh catalyst manufacturer, the specific FCC unit requirements, and the type of crude oil refined - ECat from the same refinery remains chemico-mineralogically and physically stable over extended periods of time.

Importantly, ECat exhibits high pozzolanic activity due to its substantial specific surface area (>100 m^2/g) (Sadeghbeigi , 2012; Vogt and W; uysen, 2015; Ferella et al., 2016; Rattanasak et al., 2001; Antiohos et al., 2006; Su et al., 2000; Fu et al., 2021; Zhang et al., 2021)which enable ECat's effective application as a supplementary cementitious material - replacing 10–20 % of cement or around 10 % of sand - in mortars, and concretes, typically improving their performance (Asim et al., 2021; Costa and Marques, 2018; Castellanos and Agredo, 2010) including durability (Matos et al., 2021; Costa et al., 2014a; Izquierdo et al., 2015); in specialised systems such as ultra-high-performance fiber-reinforced cementitious composites (as an internal curing agent) (Mat, et al., 2019; Huang et al., 2023), 3D-printed cementitious products (Lu et al., 2023); and in geopolymer cementless binders (as precursor) (Costa et al., 2014b; Ruiz et al., 2019; Zhang et al., 2020; Lei and Pavia, 2025). Consistent with these findings and supported by previous research conducted by the authors of this paper, a construction materials manufacturer has successfully integrated ECat into a large-scale, greener adhesive cement-based mortar formulation, thereby underscoring the by-product's considerable potential as a sustainable, reliable resource for the construction materials industry (Cimento cola WEBERCOL FLEX LEV).

A prior study has investigated the use of ECat (generated from a Spanish oil refinery) in the formulation of non-hydraulic (aerial) lime-based mortars (Arizzi and Cultrone, 2018). This research systematically compared the performance of ECat-modified mortars with those incorporating metakaolin at equivalent lime replacement levels (between 10 and 20 % by mass). The findings confirmed the pozzolanic activity of ECat, as evidenced by a subtle refinement of the pore structure in the ECat-lime binder matrix relative to the plain binder, along with an increase in compressive strength. However, in this study, ECat exhibited lower pozzolanic reactivity than metakaolin, as indicated by the same assessed properties. The study highlights the crucial role of particle size, curing conditions, and hydration mechanisms in

determining the performance of pozzolanic mortars.

Modern industrial mortar formulations present a multidimensional engineering challenge, incorporating diverse constituents - such as hydraulic binders, pozzolans, performance-enhancing admixtures, and aggregates - to satisfy workability, mechanical, durability, economic, aesthetic, regulatory, and environmental requirements. Optimising these mixtures is especially complex, as it demands comprehensive characterisation of all constituents and the assessment of their interactions while targeting often conflicting requirements.

Adopting a systematic statistical framework, such as the design of experiments (DoE), advances scientific understanding of mortars' behaviour at the system level by quantitatively capturing the main, interaction, and quadratic effects of mixture parameters (design variables) on fresh and hardened properties (response variables). This data-driven statistical methodology is both resource- and time-efficient, as it minimises the number of experimental runs while uncovering relationships not accessible through single-factor experimentation and providing evidence complementary to mechanistic and microstructural research.

Despite the growing interest in enhancing the fundamental understanding of lime-based mortars as well as in developing predictive response surface models to support multivariable optimisation of their formulations, the application of statistical methodologies such as DoE and Response Surface Methodology (RSM) remains relatively limited. Existing studies primarily focus on enhancing mechanical properties and durability in contexts such as rammed earth stabilisation (Luo et al., 2022) and lime-cement mortars incorporating industrial by-products (García-Cuadrado et al., 2017, 2018). Therefore, a comprehensive exploration of these methodologies across diverse formulations and performance criteria is still an emerging research avenue.

This research implements a systematic experimental strategy - grounded in a design of experiments (DoE) approach - to examine how fresh-state (workability) and hardened-state properties (compressive strength, ultrasound pulse velocity, and dynamic modulus of elasticity) of blended ECat-hydraulic lime mortars are influenced by three key mixture parameters (ECat-to-binder, water-to-binder, and water-repellent-to-solid ratios). Furthermore, mathematical models are developed to describe the quantitative relationship between design variables and response variables. Finally, numerical optimisation techniques are employed to determine the optimal mixture parameters that meet the performance requirements of rehabilitation mortars for various applications.

2. Materials and methods

2.1. Materials

The constituents used in the preparation of the mortars' samples consisted of: two binders, namely commercial hydraulic lime of the class HL 5 (according to the European standard EN 459-1) and ECat, generated at the fluid cracking catalytic unit of the Portuguese oil-refinery company at Sines; three limestone aggregates (two sands with distinct particles size and a filler (LF)); three admixtures; and, tap water.

Table 1 presents the bulk chemical composition of HL 5, ECat and LF as well as the pozzolanic activity of ECat. The chemical composition of each material was obtained by X-ray fluorescence spectrometry (XRF), and the loss on ignition (LOI) was determined according to the European Standard EN 196-2. The HL 5 consists mainly of CaO (53.94 %), SiO_2 (14.16 %), and Al_2O_3 (4.29 %) as expected for a hydraulic lime. The $Ca(OH)_2$ content in the HL 5 was determined by multiplying the LOI in the range 250–500 °C (5.77 %) (corresponding to the thermal decomposition of $Ca(OH)_2$) by the $Ca(OH)_2$/CaO molar mass ratio (1.32), resulting in 7.62 % by mass. This value is above the 4 % minimum set by the European Standard EN 459-1. Similarly, the $CaCO_3$ content present was determined by multiplying the LOI in the range 500–950 °C (13.24 %) (corresponding to the decomposition of $CaCO_3$) by the $CaCO_3$/CaO molar mass ratio (1.78), resulting in 23.57 % by mass. Thus, the relatively high LOI value of the HL 5 (19.98 %) is consistent with the volatiles released during these thermal decompositions, rather than with the presence of contaminants. The ECat is predominantly composed of SiO_2 (40.30 %) and Al_2O_3 (54.45 %), which is typical of pozzolanic materials. Worth noting that the LOI value of ECat complies with the limits set by standards for cementitious materials, namely EN 450 (<5 %) and EN 15167 (<3 %). As expected, the LF is mainly composed of $CaCO_3$, with a mass percentage of 77.03 % (determined using the same rationale described earlier), which accounts for its high LOI value.

Table 1
Chemical composition of the binding materials and LF as well as pozzolanic activity of ECat.

	HL 5	ECat	LF
Chemical Composition (%, by mass)			
SiO_2	14.16	40.30	0.97
Al_2O_3	4.29	54.45	0.29
Fe_2O_3	1.77	0.45	0.14
CaO	53.94	0.06	55.31
MgO	1.78	0.15	0.20
SO_3	1.90	0.00	0.05
K_2O	1.28	0.02	0.02
Na_2O	0.21	0.43	0.00
TiO_2	0.27	0.72	0.02
P_2O_5	0.05	0.50	0.00
MnO	0.03	0.00	0.01
SrO	0.05	0.00	0.01
V_2O_5	0.00	0.33	0.00
NiO	0.00	0.42	0.00
La_2O_3	0.00	0.87	0.00
LOI (110–250 °C)	0.97	–	0.04
LOI (250–500 °C)	5.77	–	0.11
LOI (500–950 °C)	13.24	–	43.28
TOTAL LOI	19.98	1.05	43.43
TOTAL	99.71	99.75	100.45
Pozzolanic Activity			
Activity Index - AI (%), 28d	–	83.6	–
Modified Chapelle test result (mg of $Ca(OH)_2$ per g of pozzolan)	–	1540	–

The pozzolanic activity of ECat was evaluated using two methods: the indirect activity index (AI) test, following European Standard EN 450-1, and the direct modified Chapelle test, as outlined in French Standard NF P 18–513. The AI was calculated as the ratio (in percentage) of the compressive strength of a mortar with a binder composed of 25 % ECat and 75 % CEM I 42.5R cement to the compressive strength of a plain cement mortar, resulting in a value of 83.6 %. This value indicates that ECat is a pozzolanic material, as it exceeds the standard threshold of AI $\geq$ 75 % for pozzolanic materials. The Chapelle test measured a consumption of 1540 mg of calcium hydroxide ($Ca(OH)_2$) per gram of ECat (i.e., 1167 mg CaO/g ECat). This value also confirms the ECat's high pozzolanicity, as it significantly exceeds the value of 660 mg of CaO/g of pozzolan set in the standard NF P 18–513 for a material to be considered pozzolanic. Moreover, the result of the Chapelle test for the ECat is also higher than many found in the literature survey for other pozzolanic materials (Quarcioni et al., 2015; Ferraz et al., 2015; Avet et al., 2016).

Fig. 1 shows backscattering electron mode (BSE) scanning electron microscopy (SEM) images of flat-polished cross-sections of ECat particles in their (a) as-received state and (b) after 28 days of exposure to a Ca$(OH)_2$ solution, as well as the energy-dispersive X-ray spectroscopy (EDS) elemental maps of Al, Si, and Ca. As shown in Fig. 1(a), the as-received ECat particles are mainly composed of Al and Si, with these chemical elements homogeneously distributed throughout the particles' matrix, consistent with the bulk chemical composition presented in Table 1. Also, as expected based on the ECat's chemical composition, Ca is absent at this stage. In contrast, Fig. 1(b) reveals that after 28 days of interaction with the $Ca(OH)_2$ solution, Ca has significantly diffused into

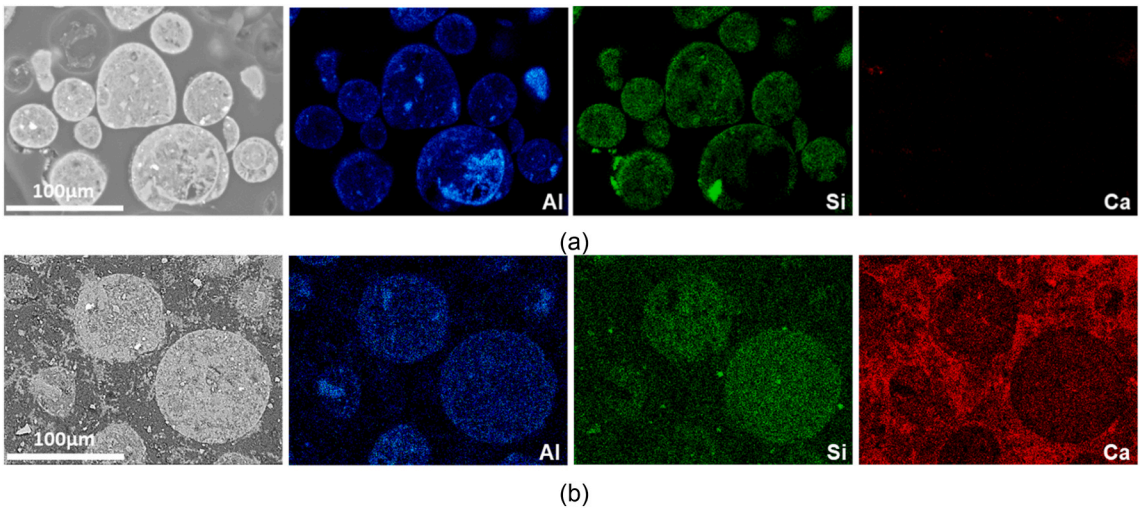

Fig. 1. BSE/SEM images from flat-polished cross-sections of ECat particles (a) as provided and (b) after 28 days of hydration in a $Ca(OH)_2$ solution, with corresponding X-ray diffraction maps of Al, Si, and Ca.

the ECat particles, providing microstructural evidence of their pozzolanic reactivity through the formation of new calcium aluminate and calcium silicate phases.

Table 2 presents the main physical properties of the binder materials and aggregates used in the mortars' preparation. The specific gravity of HL 5 was determined following the Portuguese LNEC specification E−64, that of ECat was measured by helium pycnometry, and that of LF was obtained according to European standard EN 1097-7. The specific gravities of the sands, both coarser sand (SandC) and finer (SandF), along with the 24-h water absorption (WA_{24}) of the sands and ECat were determined following the European standard EN 1097-6. The specific surface area (SSA) of the ECat was determined by nitrogen adsorption-desorption isotherm at 77 K. The particle size distributions (PSD) of HL 5, ECat and LF were obtained by laser diffraction, while the PSD of the sands and their fineness modulus were obtained using European standard EN 933-1. Fig. 2 shows the cumulative particle size distributions of all solid materials.

The physical properties of HL 5, LF, SandF and SandC fall within the typical ranges for materials used in hydraulic lime-based mortars. Only the physical properties of ECat (as mentioned elsewhere (Costa and Marques, 2018)) are particularly noteworthy. ECat exhibits a microporous structure comprising a network of interconnected tunnels and cages with strong water affinity (Sadeghbeigi, 2012; Vogt and Weckhuysen, 2015). This unique microstructure results in an exceptionally high SSA (150070 m^2/kg) - substantially greater than that of most pozzolanic materials (Avet et al., 2016) (Bumanis et al., 2020) - and a correspondingly high WA_{24} (30 %). In addition, its huge SSA is a key contributor to its remarkable pozzolanic activity (Table 1). In fact, ECat possesses the narrowest PSD among the binder and aggregate materials,

Table 2
Main physical properties of the binder materials and aggregates.

Physical Property	Binders		Aggregates		
	HL 5	ECat	LF	SandF	SandC
Specific gravity (Kg/m^3)	2640	2690	2683	2676	2692
24-h water absorption (%)	–	30	–	0.64	0.65
Specific surface area (m^2/kg)	–	150 070	–	–	–
Particle size distribution:					
Mean (µm)	24.1	91.7	7.86	–	–
d_{10}[a] (µm)	2.2	53.4	1.46	137.4	547.9
d_{50}[a] (µm)	18.8	87.3	7.03	346.7	814.22
d_{90}[a] (µm)	61.5	138.1	15.3	771.9	1143.4
Fineness modulus	–	–	–	2.9	3.2

[a] d_{10}, d_{50}, d_{90}: 10th, 50th and 90th percentiles of the distribution, respectively.

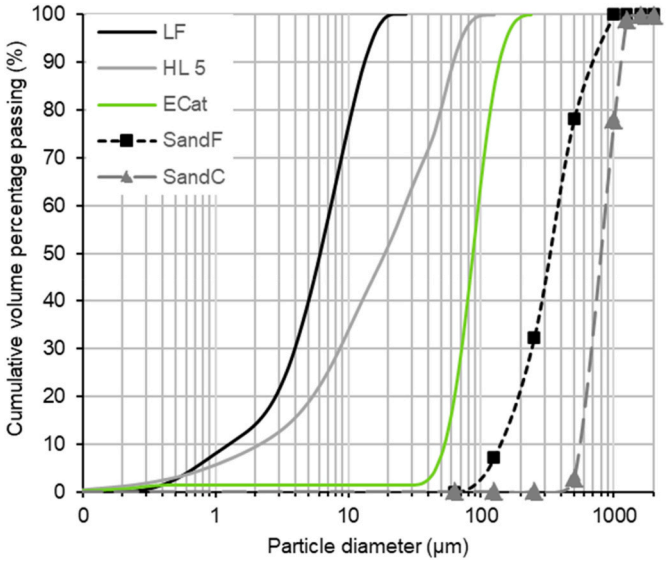

Fig. 2. Particle size distribution of the binder materials and aggregates.

with a median particle size of 87.3 µm, which is intermediate between those of LF and HL 5 and of those of the sands (Fig. 2). Therefore, since the ECat particles are coarser than those of HL5, they are unlikely to provide a significant filler effect, as their larger size limits their ability to occupy the intergranular voids between HL5 particles. Therefore, the superior strength observed in the blended ECat cement mortar (prepared to determine AI), which exceeds the value based on the dilution effect (i.e., higher than 75 %) is attributable to the ECat's pozzolanic activity, resulting in the densification of the binder mortar matrix (Cyr et al., 2006).

The admixtures used were as follows: a rheology modifier (Feng et al., 2024), an off-white powder substance based on methylcellulose derivative (with a pH of 6.5–8, at 2 % aqueous solution and a bulk density of 200–500 kg/m^3, as reported by the manufacturer); an air-entraining agent (Kontić et al., 2023), a yellow powder composed of olefin sulfonates (with a pH of 9–10.5, at 1 % aqueous solution and a bulk density of 600 kg/m^3, as reported by the manufacturer); and, a water-repellent (WR) agent, a cream coloured powder consisting of pure sodium oleate.

2.2. Design of experiments (DoE) and mixture proportions

The effects of three key mixture parameters on the properties of a commercial hydraulic lime mortar for restoration and rehabilitation were systematically investigated using a DoE technique, specifically a full factorial Central Composite Design (CCD) (Montgomery, 2012). The independent mixture variables examined were the mass percentage of ECat in the binder ($\%ECat/_{binder}$), the water-to-binder mass ratio ($w/_{binder}$) (with the binder defined as the combined mass of HL5 and ECat), and the mass percentage of water repellent in solids ($\%WR/_{solids}$).

The independent variables used in the DoE were selected because they are key parameters governing both fresh and hardened properties of lime mortars. Moreover, the $\%ECat/_{binder}$ ratio is essential for evaluating the feasibility of incorporating this industrial pozzolan, which is the main goal of this study; the $w/_{binder}$ ratio is particularly crucial for restoration lime-based binding systems because water is consumed by both hydraulic and pozzolanic reactions, is removed by evaporation and absorption into the substrate, and influences curing conditions (Alvarez et al., 2021); and, the water-repellent is one of the most expensive constituents; thus, optimising this variable also contributes to the formulation's cost-effectiveness. Aggregates-to-binder mass ratio of 3; an aggregate composition of 66.8 % SandC, 26.5 % SandF, and 6.7 % LF; and mass fractions of 0.1 % rheology modifier and 0.007 % air-entraining agent in the solids were maintained constant across all mortars, reflecting an industrial hydraulic lime mortar formulation.

The evaluated properties included workability in the fresh state, assessed through the spread flow diameter (DFlow), and compressive strength (Rc), ultrasound pulse velocity (UPV), and dynamic modulus of elasticity (Ed) at 91 days (section 2.3) in the hardened state. While the DFLow is critical for ensuring the proper workability of these mortars during application, R_c and E_d address key performance and compatibility requirements between the rehabilitation lime-based mortars and the substrate materials (Alvarez et al., 2021; Loureiro et al., 2020; Rosário Veiga et al., 2010; Dimou et al., 2022).

A full factorial CCD consists of 2^k factorial points, where k is the number of mixture variables, and the replicated central points to estimate the pure error. This design was augmented with two additional axial points along each coordinate axis, placed symmetrically placed at a distance of $\propto = (2^k)^{1/4}$ from the origin, in coded units (Montgomery, 2012). The inclusion of these additional axial points makes the CCD rotatable i.e, the variance of the predicted responses at any point is solely a function of its distance from the centre point of the design. This ensures a uniform prediction error across all points equidistant from the centre. As such, this design assigns five levels to each design variable, which in coded units are (-α, −1, 0, +1, + α). The total number of experimental runs, N, is given by $N = 2^k+2k + n_c$, where 2^k, 2k and n_c represent the number of factorial points, axial points, and replicated central points, respectively.

In the present study, with $k = 3$ and six replicated central points ($n_c = 6$), a total of $N = 2^3+2x3+6 = 20$ different experimental mixtures were prepared. Furthermore, for $k = 3$, the factorial points correspond to the vertices of the 3D-cube with factor levels of −1 and +1 in coded units. The value of α is computed as $\propto = (2^3)^{1/4} = 1.682$. Fig. 3 presents a schematic representation of the experimental plan employed in the CCD adopted.

Table 3 presents the mixture variable values of the mortars considered in the CCD plan, specifying their actual values and coded levels. A broad and high range of 20–60 % of $ECat/_{binder}$ was adopted to maximise the replacement of HL5 with ECat. This replacement range is consistent with those reported in studies using other pozzolans (Dimou et al., 2022). The experimental range for $w/_{binder}$ was set as broadly as possible, with the central point of the CCD plan yielding a DFlow of around 180 mm, as recommended by the manufacturer. Lastly, the $\%WR/_{solids}$ was defined so that the central point of the CCD plan matches the commercial reference mortar, while the domain range allowed testing mortars without WR, an expensive constituent that the manufacturer seeks to minimise.

Except for the ECat, the materials and the mixture proportions used for the mortar at the central point of the CCD replicate the industrial hydraulic lime-based mortar for restoration and rehabilitation used as a reference, which shall not be further identified due to industrial confidentiality.

The rotatable CCD is a widely utilised DoE in Response Surface Methodology (RSM), particularly when the objective is to investigate the effects of multiple factors on the responses, as it provides experimental data suitable for fitting second-order polynomial equations (Montgomery, 2012). The general form of the empirical models obtained for each selected response (in this study, each mortar property evaluated, as detailed in Section 3.3) is expressed in equation (1).

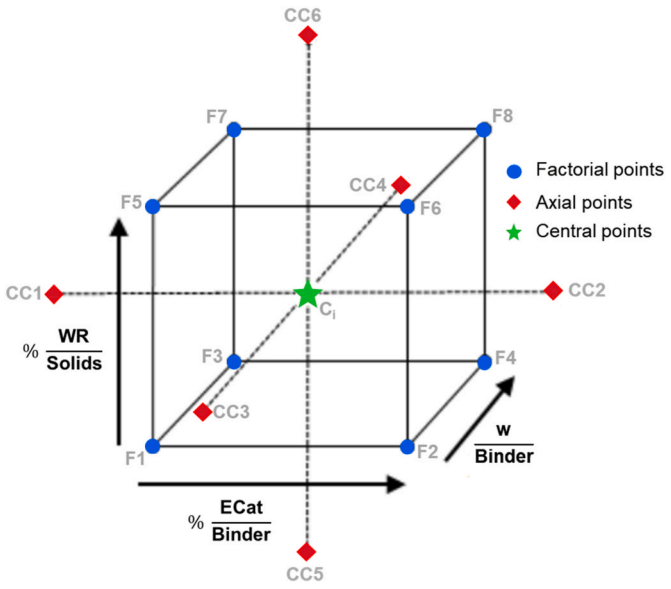

Fig. 3. Schematic representation of the three-factor full factorial CCD adopted (*Note*: The arrows indicate the increasing direction of the variable values).

Table 3
Values of mixture variables of the mortars of the CCD matrix in actual values (coded levels in parentheses).

CCD Ref.	Point type	$\%ECat/_{binder}$	$w/_{binder}$	$\%WR/_{solids}$
F1	Factorial	20 (−1)	0.95 (−1)	0.019 (−1)
F2	Factorial	60 (+1)	0.95 (−1)	0.019 (−1)
F3	Factorial	20 (−1)	1.15 (+1)	0.019 (−1)
F4	Factorial	60 (+1)	1.15 (+1)	0.019 (−1)
F5	Factorial	20 (−1)	0.95 (−1)	0.075 (+1)
F6	Factorial	60 (+1)	0.95 (−1)	0.075 (+1)
F7	Factorial	20 (−1)	1.15 (+1)	0.075 (+1)
F8	Factorial	60 (+1)	1.15 (+1)	0.075 (+1)
CC1	Axial	6.38 (−1.682)	1.05 (0)	0.047 (0)
CC2	Axial	73.6 (1.682)	1.05 (0)	0.047 (0)
CC3	Axial	40 (0)	0.8818 (−1.682)	0.047 (0)
CC4	Axial	40 (0)	1.2182 (1.682)	0.047 (0)
CC5	Axial	40 (0)	1.05 (0)	0.000 (−1.682)
CC6	Axial	40 (0)	1.05 (0)	0.094 (1.682)
C_i[(a)]	Central	40 (0)	1.05 (0)	0.047 (0)

[(a)] Central point was replicated five times.

$$Y = \beta_0 + \sum_{i=1}^{k} \beta_i X_i + \sum_{i=1}^{k} \beta_{ii} X_i^2 + \sum_{i<j} \sum \beta_{ij} X_i X_j + \varepsilon \quad (1)$$

where Y represents the predicted response (each mortar property); X_i corresponds to the independent mixture variables; and β_0, β_i, β_{ii}, β_{ij} are the regression coefficients. Specifically, β_0 is the independent term, β_i and β_{ii} represent, respectively, the linear and quadratic (second-order) effects of the independent variables on the response, and β_{ij} represents the interaction effect of the variables on the response. Finally, ε is the error term in the response accounting for random deviations not captured by the model or higher-order terms not considered.

The design of experiments, statistical analysis of experimental results, and development of mathematical models were conducted using the commercial software Design-Expert V12 (Design-Expert® software). This software facilitated the fitting of polynomial equations through regression analysis, the validation of the models via analysis of variance (ANOVA), and the optimisation of mortar compositions. A detailed description of the model identification steps can be found in (Nunes et al., 2013).

2.3. Mortars preparation and test methods

Despite using an industrially standardised hydraulic lime, it typically exhibits an inherent heterogeneity, which can lead to significant variability in the properties among mortar samples (Rosário Veiga et al., 2010). To mitigate this variability and minimise the effect of outliers, nine (9) replicate mortar samples were tested. Therefore, considering that the CCD plan included 20 different experimental mixtures (Section 2.2), and nine replicate samples were prepared for each mixture, a total of 180 samples were prepared.

The mortars were prepared in batches of 2.5 kg using a two-speed mixer (in accordance with the European Standard EN 196-1), following the mixing procedure outlined in Table 4. The preparation sequence of the mortars of the CCD plan (Fig. 3) was randomised to minimise the impact of uncontrolled variables not explicitly included in the experimental design.

Immediately after the mixing, the DFlow of the fresh mortars were measured using the flow table test, following the European standard EN 1015-3. The results were calculated as the mean of nine replicate measurements of each mixture. Subsequently, the mortars were cast into prismatic steel moulds (40x40 × 160 mm) as specified by European standard EN 1015-11. The samples were initially stored in a sealed plastic bag for 24 h and then transferred to a curing chamber at a temperature of 20 ± 2 °C and relative humidity of 95 ± 5 %. After 7 days, they were demoulded and returned to the chamber, where they remained until reaching 91 days of curing. All hardened-state properties of the mortars were assessed at this age. Two measurements were performed for each replicate mixture, resulting in a total of 18 values, with the reported results representing the average of these values.

The UPV was measured using the direct transmission method, in accordance with the European standard EN 12504-4, utilising a PROCEQ Tico test equipment equipped with two 54 kHz transducers. Measurements were conducted until two consecutive readings for the same sample differed by no more than 0.5 μs. These two readings were then recorded. The UPV values were calculated using Equation (2).

$$\mathrm{UPV} = \frac{\mathrm{L}}{T}(\mathrm{km/s}) \quad (2)$$

where L (mm) is the length of the ultrasonic pulse path between the two transducers and T (μs) is the transit time through the sample provided by the test equipment.

The E_d of the mortars was determined using Equation (3), as specified by the Brazilian standard NBR 15630.

$$E_d = UPV^2 \cdot \rho' \cdot \frac{(1+\nu)\cdot(1-2\nu)}{(1-\nu)}(\mathrm{MPa}) \quad (3)$$

where UPV is the UPV (km/s) obtained by Equation (2); ρ′ is the density of hardened mortar (kg/m^3) calculated by dividing the sample mass (measured before UPV testing) by its volume (0.256×10^{-3} m^3); and ν is the dynamic Poisson's ratio, assumed 0.2 (as recommended in the standard).

After the UPV test, the compressive strength (R_c) of the mortars was evaluated in accordance with the European standard EN 1015-11.

Table 4
Mortars mixing procedure.

Task	Time (min)
Introduce aggregates, HL5, ECat, admixtures	0
Mixing at slow speed (140 ± 5 revolutions·min^{-1})	0–4
Stop mixer; add water; manual mixing	4–5
Mixing at slow speed	5–7
Stop mixer; scrape material adhering to bowl	7–8
Mixing at slow speed	8–10
Stop mixer; scrape material adhering to bowl; resting period	10–16

3. RESULTS and discussion

3.1. Range of experimental results

Fig. 4 presents the experimental results for spread flow diameter (DFlow), compressive strength (R_c), ultrasound pulse velocity (UPV) and dynamic modulus of elasticity (E_d), at 91 days for the 20 mortar mixtures considered in the central composite design (CCD) plan (Table 3). The corresponding numerical values are provided in Supplementary Table S1.

Table 5 summarises the descriptive statistical parameters for both the central points (N = 6) and all points (N = 20) of the CCD plan. These parameters, along with the graphical representation in Fig. 4, reveal that the experimental regions adopted for the mixture variables led to wide ranges of the mortar properties. Specifically, Dflow ranges from 151 to 232 mm, R_c ranges from 0.19 to 1.52 MPa, UPV ranges from 0.82 to 1.45 km/s, and E_d ranges from 706 to 2559 MPa. Moreover, the coefficients of variation calculated for the central points (Ci), representing the experimental error of each test, are significantly lower than those obtained for the complete set of CCD plan points. Namely, the experimental error for DFlow is 1.0 % compared to a variation of 12.5 % for the complete plan points; for R_c, the values are 8.2 % versus 57.1 %; for UPV, the values are 2.6 % versus 16.8 %; and for Ed, the values are 6 % versus 38 %. These pronounced differences in the range and variability of the properties between the complete set of CCD plan points highlight the significant influence of the mixing parameters on the evaluated mortar properties. These findings indicate a substantial impact of the mixture variables, suggesting the potential for accurate empirical modelling (as verified in Table 6). In addition, the R_c and E_d results obtained with the CCD mortar mixtures fall within the ranges of values set by the European standard EN 998–1:2010 for general-purpose rendering and plastering mortars, as well as for renovation mortars (R_c ranging from 0.4 to 5.0 MPa). The results also align with the requirements for rendering and repointing substitution mortars for ancient buildings (R_c ranging from 0.4 to 5.0 MPa; E_d ranging from 2000 to 6000 MPa) (Rosário Veiga et al., 2010).

3.2. Regression models

3.2.1. Empirical fitting models and ANOVA results

To quantitatively model the influence of three mixture design parameters ($\%EC_{at}/_{binder}$, $w/_{binder}$, $\%WR/_{solids}$) on each evaluated mortar property (DFlow, R_c, UPV and E_d), a least-squares regression was conducted to fit a second-order response surface model to the experimental results (Supplementary Table S1; Fig. 4) obtained from the

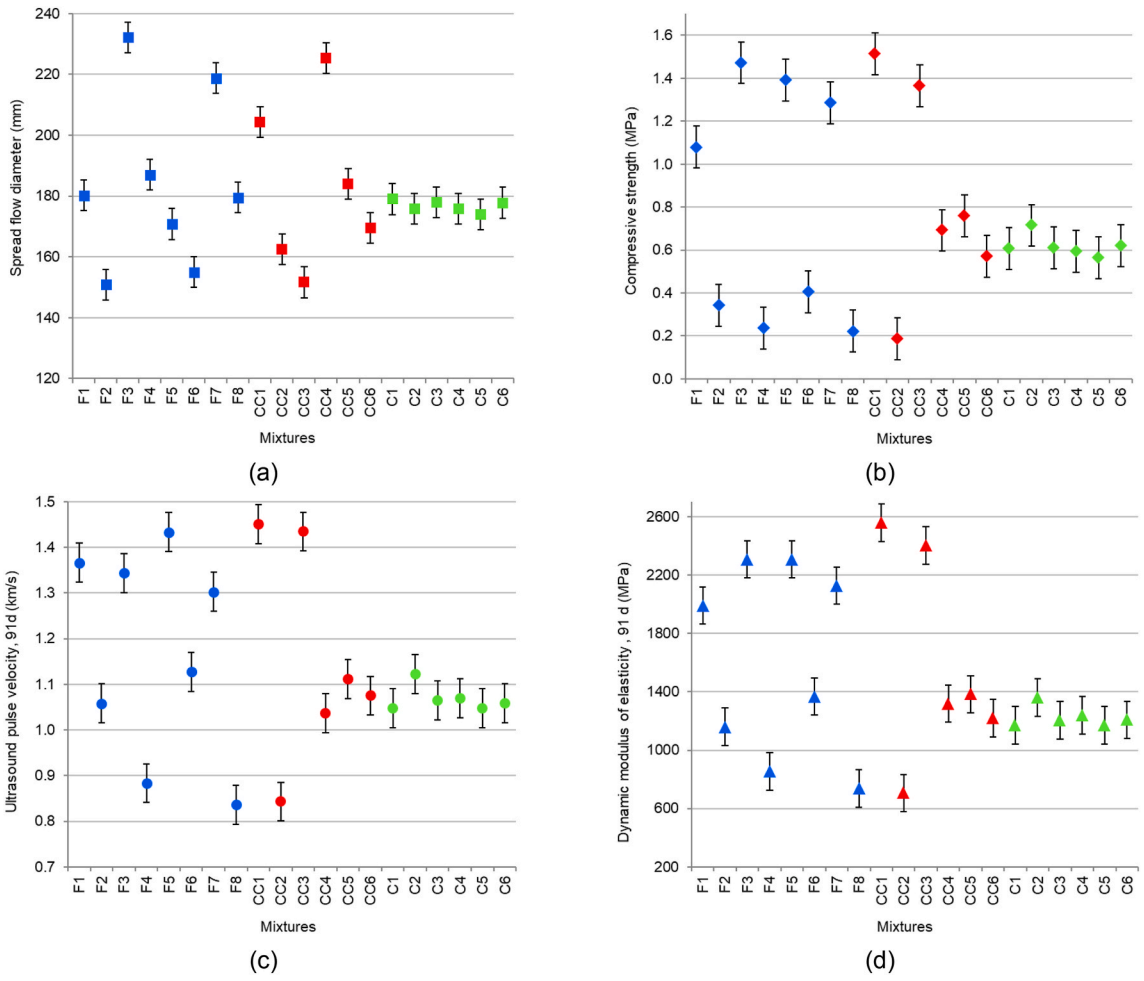

Fig. 4. Experimental results obtained for all mixtures included in the CCD experimental plan (a) DFlow (■), (b) R_c (◆); (c) UPV (●); (d) E_d (▲).

Table 5
Descriptive statistics for central points ($N = 6$) and for all data points from the CCD experimental design ($N = 20$).

	DFlow (mm)		R_c (MPa)		UPV (km/s)		E_d (MPa)	
Points considered	$N = 6$	$N = 20$	$N = 6$	$N = 20$	$N = 6$	$N = 20$	$N = 6$	$N = 20$
Minimum	174	151	0.56	0.19	1.05	0.84	1170	706
Maximum	179	232	0.71	1.52	1.12	1.45	1362	2559
Mean	182	177	0.62	0.76	1.07	1.14	1225	1490
Standard deviation	1.8	22.7	0.05	0.43	0.03	0.19	71	573
Coefficient of variation (%)	1.0	12.5	8.2	57.1	2.6	16.8	6	38

Table 6
Summary of ANOVA results for the fitted models.

Property	Model	Variable transformation	*p*-value	*p*-value for lack of fit	Error term (ε)[a]		
					Std.Dev.	R^2	R^2_{Adj}
Dflow	Quadratic	none	<0.0001	0.061	2.51 mm	0.988	0.981
Rc	Quadratic	$1/\sqrt{R_c}$	<0.0001	0.086	0.070 (0.090 MPa)[b]	0.975	0.966
UPV	Quadratic	1/UPV	<0.0001	0.813	0.015 (0.019 km/s)[b]	0.990	0.985
E_d	Quadratic	$1/E_d$	<0.0001	0.109	0.506×10^{-4} (139 MPa)[b]	0.968	0.945

[a] Error term is a random and normally distributed variable with mean zero.
[b] Standard deviation in the original scale.

mixtures designed using the CCD approach (Section 2.2).

An iterative backwards elimination process was used to enhance the accuracy of each property model. The modelling procedure started with fitting a full second-order polynomial model to the experimental results. Thereafter, the significance of each design mixture variable for each property was evaluated using a Student's t-test at a 95 % confidence

level. Accordingly, design variables with p-values greater than 0.05 were considered non-significant and were sequentially removed from the model, starting with the variable with the highest *p*-value. This elimination process was repeated iteratively, with the model being refitted after each removal, until only significant variables (p-value <0.05) remained. To maintain model hierarchy and ensure its interpretability, any non-significant first-order terms were retained if their associated second-order terms were significant. When residual analysis indicated model inadequacy or violations of normality assumptions, appropriate transformations were applied to the response variables. Specifically, the inverse square-root $\left(1/\sqrt{y}\right)$ transformation was used for R_c, while the inverse transformation $\left(1/y\right)$ was employed for UPV and E_d models.

Table 6 summarises the ANOVA results for the fitted models obtained. All regression models presented high statistical significance, as their p-values are much smaller than 0.05, specifically smaller than 10^{-4}. Moreover, the lack-of-fit tests were not significant for any of the models relative to their pure errors, as indicated by corresponding p-values exceeding 0.05. For all models, Variance Inflation Factor (VIF) values were approximately 1.0, indicating no evidence of multicollinearity among the predictor variables. The high values of both the predicted (R^2 >0.968) and adjusted (R^2_{Adj} >0.945) regression coefficients suggest that a substantial proportion of the variability in the experimental results for each mortar property is explained by the respective regression models. Furthermore, the minimal difference between the R^2 and the R^2_{Adj} values (specifically, 0.005 for the R_c and UPV models, and 0.004 for the E_d model) indicates that the models do not include unnecessary terms, thereby ensuring that they are not overfitted.

Table 7 presents the regression models expressed in terms of coded values, allowing for a direct comparison of the magnitude of the model coefficients to assess the relative effects of each parameter on the properties. As such, larger coefficient values indicate a greater influence of the mixture variable on the property, while positive coefficients indicate that the property (or transformed response) value increases with an increase in the mixture parameter, and negative coefficients indicate the opposite effect. For each model, which is valid for mixture parameters within the ranges specified in Table 3, the three most significant parameters are highlighted in bold, with the most significant term additionally underlined.

The coefficients of the regression models (Table 7) clearly indicate that the ECat incorporation level in the binder exerts a substantial effect on all evaluated mortar properties. Namely, the $\%ECat/_{binder}$ ratio is the most significant parameter influencing the hardened state properties R_c, UPV, and E_d, and it is the second most important design variable for the DFlow model, which for this property is only surpassed by the effect of w/binder. Additionally, the interaction between $\left(\%ECat/_{binder}\right) \times \left(w/_{binder}\right)$ is also among the three most significant variables across all models. In contrast, the WR content level is the mixture variable with the least effect on the assessed mortar properties, both independently and in its interactions with other parameters, as indicated by its minimal coefficient values.

The presence of significant regression coefficients for the quadratic (β_{ii}) and interaction (β_{ij}) terms (equation (1)) indicates that the models exhibit curvature, reflecting the nonlinear and interaction effects between factors (mixture variables) and the response variables (properties). These findings not only confirm the complexity of the system under study but also validate the appropriateness of adopting a CCD-based DoE to obtain models that accurately represent the underlying response surface. More details on the individual and interaction effects of mixture variables on the mortar properties are presented in section 3.2.2.

3.2.2. Individual and interaction effects of mixture variables on the properties

Fig. 5 presents the contour and 3D-response surface plots of the mortars' properties evaluated in this investigation as functions of $\%ECat/_{binder}$ and $w/_{binder}$ within their respective domain ranges (Table 3). Since the design variable $\%WR/_{solids}$ exhibited a minimal effect on the mortars' properties (Table 7), its value was kept constant at 0.047 %, corresponding to the midpoint of its experimental range.

Fig. 5(a) shows that over their domain ranges, the individual variables $\%ECat/_{binder}$ and $w/_{binder}$ generally lead to opposite effects on the DFlow of the fresh state mortars: increasing the $\%ECat/_{binder}$ tends to reduce DFlow, whereas conversely, increasing $w/_{binder}$ raises it. In addition, the figure also confirms the interaction effect between these two variables on DFlow, as identified by the mathematical model (Table 7). Namely, at lower $w/_{binder}$ ratios, DFlow values are smaller and exhibit less sensitivity to changes in $\%ECat/_{binder}$, whereas at higher $w/_{binder}$ ratios, DFlow becomes more responsive to variations of the ECat replacement level.

Table 7
Fitted regression models (in coded variables).

	DFlow (mm)	$1/\sqrt{Rc}$ ($MPa^{-1/2}$)	$1/_{UPV}$ (s/km)	$1/_{E_d}$ x10^{-4} (1/MPa)
Independent	177	1.28	0.929	8.60
$\%ECat/_{binder}$	**−14.6**	**<u>0.471</u>**	**<u>0.150</u>**	**<u>2.680</u>**
$w/_{binder}$	**<u>20.8</u>**	0.101	**0.0751**	0.830
$\%WR/_{solids}$	−3.68	*NS*	0.00220 (*)	−0.110 (*)
$\left(\%ECat/_{binder}\right) \times \left(w/_{binder}\right)$	**−4.91**	**0.125**	**0.0515**	**1.63**
$\left(\%ECat/_{binder}\right) \times \left(\%WR/_{solids}\right)$	2.44	*NS*	NS	0.530
$\left(w/_{binder}\right) \times \left(\%WR/_{solids}\right)$	*NS*	*NS*	0.0208	**0.950**
$\left(\%ECat/_{binder}\right)^2$	2.55	**0.118**	*NS*	0.390
$\left(w/_{binder}\right)^2$	4.36	−0.0672	0.0208	−0.730
$\left(\%WR/_{solids}\right)^2$	*NS*	*NS*	−0.0373	*NS*

NS – Non-significant term.
(*) – Term non-significant that remained in the model to keep its hierarchy.
The three most significant parameters are typed in bold, and the most significant term is also underlined.

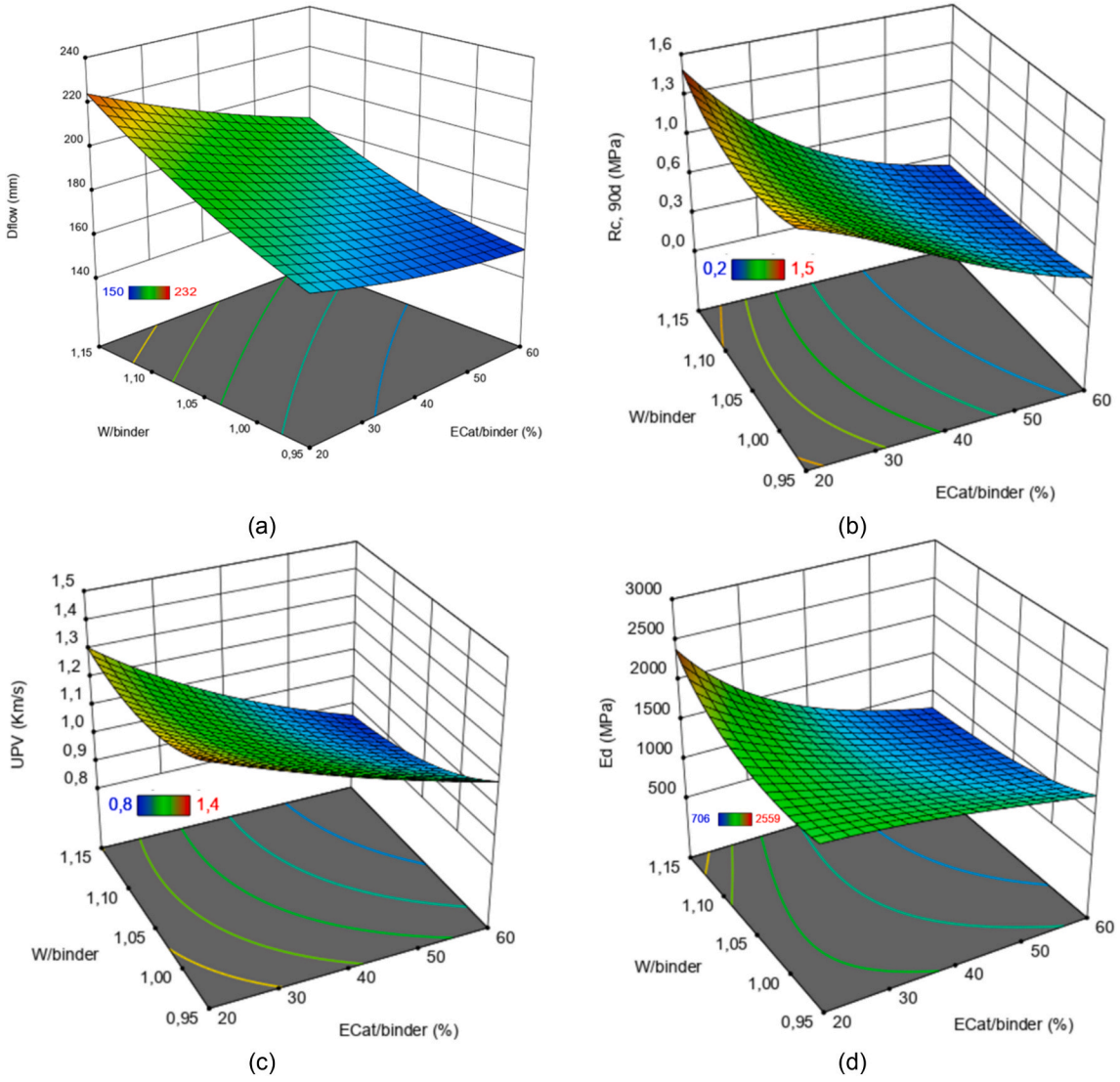

Fig. 5. Contour and 3D response surface plots of (a) DFlow, (b) *Rc*; (c) UPV, and (d) E_d (using actual variables) as functions of $\%ECat/_{binder}$ and $w/_{binder}$, with $\%WR/_{solids}$ fixed at 0.047 %.

These results are consistent with previous studies reporting that higher $w/_{binder}$ ratios in lime-based mortars generally increase workability, resulting in larger DFlow (Hanley and Pavía, 2008; Pavía and Hanley, 2010). Moreover, the cross-effect of the pozzolan content and $w/_{binder}$ ratio on the DFlow corroborates the findings of (Pavía and Hanley, 2010), who observed that at lower $w/_{binder}$ ratios, mortars are stiffer and less affected by increasing the pozzolan content.

Fig. 5(b–d) show that individually increasing the $w/_{binder}$ ratio tends to decrease all hardened-state properties (R_c, UPV and E_d). Likewise, raising the $\%ECat/_{binder}$ ratio alone also leads to lower these properties, corroborating regression models' findings (Table 7). Furthermore, these figures highlight the cross-interaction $w/_{binder}$ and the $\%ECat/_{binder}$. Although the magnitude of the effects differs, the overall trend is consistent: at higher $w/_{binder}$ ratios, the property values tend to be lower, and the effect of $\%ECat/_{binder}$ is more pronounced than at lower $w/_{binder}$ ratios. This indicates that at lower $w/_{binder}$ ratios, mortars are more robust regarding ECat incorporation, particularly the E_d.

The findings shown in Fig. 5(b) are consistent with previous research demonstrating that higher $w/_{binder}$ ratios in lime-based mortars reduce compressive strength (B. et al., 2023). The authors of (B. et al., 2023) attributed this trend to an increase in porosity, mainly associated with larger capillary pores resulting from higher water content.

In this investigation, the domain range for the $\%ECat/_{binder}$ ratio was set at 20–60 % (Table 3). As mentioned in the Introduction (Section 1), above a certain threshold of pozzolan content, the compressive strength may decrease. Nonetheless, the relatively high and broad range of $\%ECat/_{binder}$ was deliberately chosen to maximise by-product incorporation, despite the potential trade-off in mechanical properties - an acceptable compromise given that typical rehabilitation applications are less demanding in terms of strength requirements (Rodrigues and Grossi, 2007). Thus, the observed decrease in compressive strength with increasing $\%ECat/_{binder}$ is consistent with some previous studies on pozzolan-lime mortars (Malathy et al., 2023a; Bakolas and Aggelakopoulou, 2019; Cizer et al., 2010). Moreover, because the trends of UPV and *Ed* typically follow the compressive strength development, the observed decreases in these properties Fig. 5(c and d), also corroborate existing knowledge (Ramesh et al., 2019; Marques et al., 2020; Nalon et al., 2021).

While previous studies (Malathy et al., 2023b; Pavía et al., 2014) have suggested that a mortar's $w/_{binder}$ ratio and pozzolan content (in

Table 8
Multi-objective optimisation constraints (design variables in coded values), optimised mortars composition and respective predicted properties.

			General purpose mortar	Renovation mortar	Rendering - Ancient Build	Repointing - Ancient Build
OPTIMISATION CONSTRAINTS						
Design variables	$\%_{\frac{ECat}{binder}}$		← Maximise →			
	$\frac{w}{binder}$		In range(i)	In range(i)	In range(i)	In range(i)
	$\%_{\frac{WR}{solids}}$		In range(i)	In range(i)	In range(i)	In range(i)
Model responses	DFlow (mm)		← Range [160–180] →			
	Rc (MPa)		>0.4	Range [1.5–5.0]	Range [0.4–2.5]	Range [0.6–3.0]
	UPV (km/s)		None	None	None	None
	E_d (MPa)		None	None	Range [2000–5000]	Range [3000–6000]
OPTIMISED MORTARS						
Optimised mixture variables	$\%_{\frac{ECat}{binder}}$		56.6	38.2	34.0	24.8
	$\frac{w}{binder}$		0.982	0.858(ii)	0.985	0.961
	$\%_{\frac{WR}{solids}}$		0.000(ii)	0.000(ii)	0.103(ii)	0.103(ii)
	d(iii)		1.99	2.55	2.12	2.32
Predicted mortars' properties	DFlow (mm)	Predicted mean	160	160	160	160
		95 % PI Interval	[151–169]	[150–170]	[152–168]	[151–169]
	Rc (MPa)	Predicted mean	0,40	1.54	0.88	1.18
		95 % PI Interval	[0.320–0.517]	[0,89–3.04]	[0.63–1.25]	[0.80–1.83]
	UPV (km/s)	Predicted mean	1.02	1.42	1.24	1.39
		95 % PI Interval	[0.974–1.08]	[1.28–1.58]	[1.17–1.32]	[1.29–1.50]
	E_d (MPa)	Predicted mean	1080	1400	2030	3110
		95 % PI Interval	[888–1360]	[1010–2250]	[1450–3200]	[1810–8520]

(i)Within the range of [-2, +2], in coded values.
(ii)Optimised value outside the design domain range adopted in the models.
(iii)*d* – Euclidean distance to the center of the CCD plan.

this case, $\%ECat_{/binder}$) have a synergistic influence on its hardened-state properties (as shown in Fig. 5(b–d)), the mathematical models derived in this investigation (Table 7) offer an unbiased confirmation and quantification of these cross-effects.

3.3. Multi-objective mortars optimisation

The RSM using the desirability function approach (available in the commercial software mentioned in section 2.2) was applied to numerically optimise the composition of four ECat-lime blended mortars, addressing simultaneously eco-sustainability, cost minimisation and multiple engineering properties.

Table 8 presents the constraints used in the multi-objective optimisation scenarios, the design variables obtained for the optimised mortars, and their predicted properties. The primary goals for these mortars were to enhance eco-efficiency and reduce costs. Since ECat is an industrial byproduct generated in the fluid catalytic cracking units of oil refineries, incorporating higher levels of ECat in the binder promotes its reuse and its diversion from landfills, while also lowering mortars' costs, fulfilling both main objectives. Moreover, lime mortar manufacturers have indicated that a DFlow between 160 and 180 mm meets industrial requirements, as these values facilitate mortar application and help produce uniform layers that enhance both structural integrity and aesthetic quality. For these reasons, maximising the design variable $\%ECat_{/binder}$ and targeting DFlow within the above-mentioned range are shared optimisation goals across all the scenarios.

Two of these scenarios aim to optimise general-purpose mortars and renovation mortars, as defined in the European Standard EN 998–1:2010, which specifies requirements for masonry rendering and plastering. Namely, general-purpose mortars (fourth column in Table 8) require R_c higher than 0.4 MPa, whereas renovation mortars (fifth column) require R_c values from 1.5 to 5.0 MPa.

The remaining two optimisation scenarios (sixth and seventh columns) address substitution mortars applied in rendering ($R_c \in [0.4–2.5]$ MPa; $E_d \in [2000–5000]$ MPa) and repointing ($R_c \in [0.6–3.0]$ MPa; $E_d \in [3000–5000]$ MPa) for ancient buildings. These limits stem from previous research on the compatibility and durability of lime-based mortars in historical buildings (Rosário Veiga et al., 2010), where R_c must remain below the substrate's strength to prevent damage, and E_d must provide the necessary flexibility to accommodate structural movement without inducing excessive stress.

The design variables $\%ECat_{/binder}$, $w_{/binder}$ and $\%WR_{/solids}$ were set to be within the range of [−2, +2] in coded values to ensure that the optimisation remains within a reasonable extrapolation limit, maintaining the reliability of the predictions. This constraint was validated after obtaining the Euclidean distances of the optimal mixtures to the center of the CCD plan (calculated as $d = \sqrt{\sum_{i=1}^{3} x_i^2}$, where x_i are the coded values of the mixture variables), because they were all less than or equal to 2.55 (Table 8). The lower and higher weight values of all constraints were both set equal to 1, and their importance was set equally.

The optimised solutions (Table 8) confirmed the feasibility of formulating eco-efficient hydraulic lime mortars with a significant content of ECat, ranging from 24.8 to 56.6 %, while still meeting the

technological requirements set by the industry and the engineering properties prescribed in both standards and literature. In particular, the optimised compositions for general-purpose rendering and masonry renovation applications support the highest replacement levels of the HL 5 with ECat (38.2–56.6 %) and do not require the inclusion of WR, as expected by the limited influence of the $\%WR_{/solids}$ variable on the mortars properties (Table 7). In addition to simplifying formulation, this omission also contributes to more cost-effective solutions.

In contrast, mortars intended for historic building rendering and repointing applications have lower ECat content (24.8–34.0 %) and demand the inclusion of WR (optimal $\%WR_{/solids}$ ratio of 0.103) to meet the E_d values required for these applications (2000–6000 MPa, Table 8). These results are consistent with the empirical model's (section 3.2.2), which shows that achieving higher E_d values imposes lowering the ECat content and also in WR presence. In fact, while the first-order term of $\%WR_{/solids}$ is not statistically significant in the E_d, regression model, significant interactions, namely between $\left(w_{/binder}\right) \times \left(\%WR_{/solids}\right)$ and $\left(\%ECat_{/solids}\right) \times \left(\%WR_{/solids}\right)$ reveal synergistic effects (Table 7) that reinforce the importance of optimising the WR.

4. Conclusions

This investigation reveals the feasibility of producing large-scale, eco-friendly hydraulic lime mortars with a significant incorporation of a by-product from the oil-refinery, ECat (up to approximately 56 % by mass), while still meeting relevant regulatory and technological requirements for masonry applications. This approach reduces reliance on hydraulic lime - produced through a resource-, energy- and carbon-intensive process - and repurposes an industrial by-product that would otherwise be landfilled. In addition, this strategy promotes other industrial symbiosis with economic benefits for both the construction and oil-refinery sectors by decreasing product costs (due to reduced lime usage) and valorising a residue.

The DoE approach employed enabled the development of robust empirical models that correlate key mixture parameters ($\%ECat_{/binder}$, $w_{/binder}$, and $\%WR_{/solids}$) with mortar properties in both the fresh (DFlow) and hardened (R_c, UPV, and E_d) states. These models enable the tailored formulation of mortars for specific applications, optimising their compatibility with modern and heritage buildings as well as increasing fundamental understanding of the effect of ECat on lime-based mortars. The principal findings include:

- Fresh-state behaviour:
  - o DFlow value is mainly determined by the $w_{/binder}$ ratio, with workability increasing as $w_{/binder}$ increases
  - o The second most influential variable is the $\%ECat_{/binder}$; however, increasing ECat content results in Dflow reduction
  - o The sensitivity of DFlow to changes in $\%ECat_{/binder}$ ratio; it lowers at reduced $w_{/binder}$ ratios, due to the cross-effect between these two design variables
- Hardened-state properties:
  - o R_c, UPV, and E_d values are mainly determined by $\%ECat_{/binder}$ ratio, decreasing when the ECat content increases
  - o Again, due to $ECat_{/binder}$ and $w_{/binder}$ cross-effect, hardened-state properties, mainly E_d, are more robust regarding ECat incorporation at lower $w_{/binder}$ ratios
  - o $\%WR_{/solids}$ ratio is the least influential variable on the assessed mortar properties, both independently and in its interactions with other parameters.

Future studies should expand the evaluated properties (e.g., water capillarity absorption, water vapour permeability, freeze-thaw resistance, carbonation rates) as well as assess the compatibility with diverse masonry substrates. Additionally, scaling up production and conducting field trials would provide critical insights into the practical implementation of these eco-efficient mortars, further advancing the understanding of ECat reuse in hydraulic lime-based mortars that can be extrapolated to other pozzolanic waste materials.

The key outcome of this investigation is the demonstration that the combined use of ECat and a CCD-based DoE methodology provides a robust framework for designing sustainable hydraulic lime mortars for building rehabilitation. This approach mitigates the environmental impacts of the construction sector, promotes the circular economy and supports innovative practices that enhance the competitiveness of the building materials industry.

CRediT authorship contribution statement

Carla Costa: Conceptualization, Formal analysis, Investigation, Methodology, Resources, Validation, Writing – original draft, Writing – review & editing. **Sandra Nunes:** Formal analysis, Methodology, Validation, Writing – review & editing.

Declaration of competing interest

The authors declare that they have no known competing financial interests or personal relationships that could have appeared to influence the work reported in this paper.

Acknowledgements

The authors gratefully acknowledge Sines Refinery (Galp Energia) for supplying ECat and CIMPOR Argamassas S.A. for providing the hydraulic lime, aggregates, and admixtures.

Appendix A. Supplementary data

Supplementary data to this article can be found online at https://doi.org/10.1016/j.dibe.2026.100860.

Data availability

Data is supplied in an .xls file included as supplementary material.

References

Agência Portuguesa do Ambiente, 2019. Declaração De Subproduto n.18/2019 [Subproduct Declaration No. 18/2019].

Aškrabić, M., Vyšvařil, M., Zakić, D., Savić, A., Stevanović, B., 2021. Effects of natural zeolite addition on the properties of lime putty-based rendering mortars. Constr. Build. Mater. 270, 121363. https://doi.org/10.1016/J.CONBUILDMAT.2020.121363.

Alvarez, J.I., Veiga, R., Martínez-Ramírez, S., Secco, M., Faria, P., Maravelaki, P.N., Ramesh, M., Papayianni, I., Válek, J., 2021. RILEM TC 277-LHS report: a review on the mechanisms of setting and hardening of lime-based binding systems. Mater. Struct. 54 (2), 1–30. https://doi.org/10.1617/S11527-021-01648-3.

Antiohos, S.K., Chouliara, E., Tsimas, S., 2006. Re-use of spent catalyst from oil-cracking refineries as supplementary cementing material. China Particuology 4, 73–76. https://doi.org/10.1016/S1672-2515(07)60238-3.

Arizzi, A., Cultrone, G., 2018. Comparing the pozzolanic activity of aerial lime mortars made with metakaolin and fluid catalytic cracking catalyst residue: a petrographic and physical-mechanical study. Constr. Build. Mater. 184, 382–390. https://doi.org/10.1016/J.CONBUILDMAT.2018.07.002.

Asim, N., Badiei, M., Torkashvand, M., Mohammad, M., Alghoul, M.A., Gasaymeh, S.S., Sopian, K., 2021. Wastes from the petroleum industries as sustainable resource materials in construction sectors: opportunities, limitations, and directions. J. Clean. Prod. 284, 125459. https://doi.org/10.1016/j.jclepro.2020.125459.

Avet, F., Snellings, R., Alujas Diaz, A., Ben Haha, M., Scrivener, K., 2016. Development of a new rapid, relevant and reliable (R3) test method to evaluate the pozzolanic reactivity of calcined kaolinitic clays. Cement Concr. Res. 85, 1–11. https://doi.org/10.1016/J.CEMCONRES.2016.02.015.

B, A., Silva, A.P., Ferreira Pinto, A., Gomes, Candeias, A., Silva, B.A., Ferreira Pinto, A.P., Gomes, A., Candeias, A., 2023. Influence of water content and mixing conditions on

the properties of lime-based materials. Buildings 13, 1530. https://doi.org/10.3390/BUILDINGS13061530.
Bakolas, A., Aggelakopoulou, E., 2019. Pozzolanic activity of natural pozzolan–lime pastes and physicomechanical characteristics. J. Therm. Anal. Calorim. 135, 2953–2961. https://doi.org/10.1007/s10973-018-7612-1.
Bošković, I., Radivojević, A., 2024. Life cycle assessment of hemp-lime concrete wall constructions: the impact of wall finish type and renewal regimes. J. Build. Eng. 86, 108940. https://doi.org/10.1016/J.JOBE.2024.108940.
Bumanis, G., Vitola, L., Stipniece, L., Locs, J., Korjakins, A., Bajare, D., 2020. Evaluation of Industrial by-products as pozzolans: a road map for use in concrete production. Case Stud. Constr. Mater. 13, e00424. https://doi.org/10.1016/J.CSCM.2020.E00424.
Cachim, P., Velosa, A.L., Rocha, F., 2010. Effect of Portuguese metakaolin on hydraulic lime concrete using different curing conditions. Constr. Build. Mater. 24, 71–78. https://doi.org/10.1016/j.conbuildmat.2009.08.010.
Castellanos, N.T., Agredo, J.T., 2010. Using spent fluid catalytic cracking (FCC) catalyst as pozzolanic addition — a review. Ing. Invest. 30, 35–42.
Cimento cola WEBERCOL FLEX LEV | Leroy Merlin, (n.d.). https://www.leroymerlin.pt/produtos/cimento-cola-webercol-flex-lev-82666276.html?gclid=CjwKCAjw1YCkBhAOEiwA5aN4AYI–s2-a09s2PJWmPUiiamPbOrRkdx6ss5DoPwEnFPHUtn4s0q5gxoCT_kQAvD_BwE (accessed February 3, 2025).
Cizer, Ö., Van Balen, K., Van Gemert, D., 2010. Competition between hydration and carbonation in hydraulic lime and lime-pozzolana mortars. Adv. Mater. Res. 133–134, 241–246. https://doi.org/10.4028/WWW.SCIENTIFIC.NET/AMR.133-134.241.
Costa, C., Ferreira, C., Ribeiro, M.F., Fernandes, A., 2014b. Alkali-activated binders produced from petrochemical fluid catalytic cracking catalyst waste. Int J Res Eng Technol 03 114–122. https://doi.org/10.15623/ijret.2014.0325019.
Costa, C., Ribeiro, M.S., Brito, N., 2014a. Effect of waste oil-cracking catalyst incorporation on durability of mortars. Mater. Sci. Appl. 5, 905–914. https://doi.org/10.4236/msa.2014.513092.
Costa, C., Marques, J.C., 2018. Feasibility of eco-friendly binary and ternary blended binders made of fly-ash and oil-refinery spent catalyst in ready-mixed concrete production. Sustainability 10, 3136. https://doi.org/10.3390/su10093136.
Cyr, M., Lawrence, P., Ringot, E., 2006. Efficiency of mineral admixtures in mortars: quantification of the physical and chemical effects of fine admixtures in relation with compressive strength. Cement Concr. Res. 36, 264–277. https://doi.org/10.1016/J.CEMCONRES.2005.07.001.
Design-Expert® software, version 12, Stat-Ease, Inc., Minneapolis, MN, USA, www.statease.com, (n.d.).
Dimou, A.E., Metaxa, Z.S., Kourkoulis, S.K., Karatasios, I., Alexopoulos, N.D., 2022. Tailoring the binder matrix of lime-based binders for restoration interventions with regard to mechanical compatibility. Constr. Build. Mater. 315, 125717. https://doi.org/10.1016/J.CONBUILDMAT.2021.125717.
European Commission, 2020. A New Circular Economy Action Plan: for a Cleaner and More Competitive Europe. Publications Office of the European Union. https://op.europa.eu/en/publication-detail/-/publication/6e6be661-6414-11ea-b735-01aa75ed71a1/language-en. (Accessed 7 February 2025).
European Lime Association, 2021. Lime as a Natural Carbon Sink. EuLA, Brussels. https://eula.eu/wp-content/uploads/2023/11/EuLA-Carbonation-Booklet_32xA4_EN_20211125.pdf.
European Parliament and Council, 2008. Directive 2008/98/EC on waste and repealing certain Directives. Off. J. Eur. Union. https://eur-lex.europa.eu/eli/dir/2008/98/oj/eng. (Accessed 7 February 2025).
Feng, K., Ma, K., Yang, H., Long, G., Xie, Y., Zeng, X., Tang, Z., Usman, I.U., 2024. Influence of cellulose ethers on rheological properties of cementitious materials: a review. J. Build. Eng. 95, 110347. https://doi.org/10.1016/J.JOBE.2024.110347.
Ferella, F., D'Adamo, I., Leone, S., Innocenzi, V., De Michelis, I., Vegliò, F., 2019. Spent FCC E-Cat: towards a circular approach in the oil refining industry. Sustainability 11, 113. https://doi.org/10.3390/su11010113.
Ferella, F., Innocenzi, V., Maggiore, F., 2016. Oil refining spent catalysts: a review of possible recycling technologies. Resour. Conserv. Recycl. 108, 10–20. https://doi.org/10.1016/j.resconrec.2016.01.010.
Ferraz, E., Andrejkovičová, S., Hajjaji, W., Velosa, A.L., Silva, A.S., Rocha, F., 2015. Pozzolanic activity of metakaolins by the French standard of the modified Chapelle test: a direct methodology. Acta Geodyn. Geomater. 12, 289–298. https://doi.org/10.13168/AGG.2015.0026.
Fu, H., Chen, Y., Liu, T., Zhu, X., Yang, Y., Song, H., 2021. Research on hazardous waste removal management: identification of the hazardous characteristics of fluid catalytic cracking spent catalysts. Molecules 26, 2289. https://doi.org/10.3390/MOLECULES26082289.
García-Cuadrado, J., Rodríguez, A., Cuesta, I.I., Calderón, V., Gutiérrez-González, S., 2017. Study and analysis by means of surface response to fracture behavior in lime-cement mortars fabricated with steelmaking slags. Constr. Build. Mater. 138, 204–213. https://doi.org/10.1016/J.CONBUILDMAT.2017.01.122.
García-Cuadrado, J., Santamaría-Vicario, I., Rodríguez, A., Calderón, V., Gutiérrez-González, S., 2018. Lime-cement mortars designed with steelmaking slags as aggregates and validation study of their properties using mathematical models. Constr. Build. Mater. 188, 210–220. https://doi.org/10.1016/J.CONBUILDMAT.2018.08.093.
Grist, E.R., Paine, K.A., Heath, A., Norman, J., Pinder, H., 2015. The environmental credentials of hydraulic lime-pozzolan concretes. J. Clean. Prod. 93, 26–37. https://doi.org/10.1016/J.JCLEPRO.2015.01.047.
Hanley, R., Pavía, S., 2008. A study of the workability of natural hydraulic lime mortars and its influence on strength. Materials and Structures/Materiaux et Constructions 41, 373–381. https://doi.org/10.1617/S11527-007-9250-0/TABLES/6.
Huang, Y., Jiao, Y., Wei, T., Li, Y., Yang, G., Yang, R., Yu, R., Wang, Z., Xiao, R., Xie, G., 2023. Study of the spent catalysts as internal curing agents on the hydration kinetics and microstructure development of ultra-high performance concrete (UHPC). Constr. Build. Mater. 409, 134027. https://doi.org/10.1016/J.CONBUILDMAT.2023.134027.
Izquierdo, S., Rodríguez, E., Mejía de Gutiérrez, R., 2015. Resistencia a la corrosión ácida de morteros de cementos adicionados con catalizador de craqueo catalítico gastado (sFCC). Revista Ingeniería de Construcción 30, 169–176. https://doi.org/10.4067/S0718-50732015000300002.
Kang, S.H., Lee, S.O., Hong, S.G., Kwon, Y.H., 2019. Historical and scientific investigations into the use of hydraulic lime in Korea and preventive conservation of historic masonry structures. Sustainability 11, 5169. https://doi.org/10.3390/SU11195169.
Kontić, A., Vasconcelos, G., Briceño Melendez, C., Azenha, M., Sokolović, N., 2023. Influence of air entrainers on the properties of hydrated lime mortars. Constr. Build. Mater. 403, 132968. https://doi.org/10.1016/J.CONBUILDMAT.2023.132968.
Lei, Z., Pavia, S., 2025. Geopolymer based on spent fluid catalytic cracking catalyst: design optimisation and high-temperature resistance. Case Stud. Constr. Mater., e04395 https://doi.org/10.1016/J.CSCM.2025.E04395.
Leone, S., Ferella, F., Innocenzi, V., De Michelis, I., Vegliò, F., 2018. Synthesis and characterization of zeolites from spent FCC catalysts. Chem Eng Trans 67, 601–606. https://doi.org/10.3303/CET1867101.
Loke, M.E., Pallav, K., Cultrone, G., Di Filippo, C., 2024. Investigating the standard design and production procedure of heritage mortars for compatible and durable masonry restoration. J. Build. Eng. 94, 110012. https://doi.org/10.1016/J.JOBE.2024.110012.
Loureiro, A.M.S., Paz, S.P.A., Veiga, M. do R., Angélica, R.S., 2020. Assessment of compatibility between historic mortars and lime-METAKAOLIN restoration mortars made from amazon industrial waste. Appl. Clay Sci. 198, 105843. https://doi.org/10.1016/J.CLAY.2020.105843.
Lu, B., Li, H., Li, M., Wong, T.N., Qian, S., 2023. Mechanism and design of fluid catalytic cracking ash-blended cementitious composites for high performance printing. Addit. Manuf. 61, 103286. https://doi.org/10.1016/J.ADDMA.2022.103286.
Luo, Y., Zhong, H., Bao, F., Guo, Z., Ni, P., 2022. Insights into natural and carbonation curing of ancient Chinese rammed earth mixed with brown sugar. Constr. Build. Mater. 317, 125969. https://doi.org/10.1016/J.CONBUILDMAT.2021.125969.
Malathy, R., Shanmugam, R., Chung, I.-M., Kim, S.-H., Prabakaran, M., 2022. Mechanical and microstructural properties of composite mortars with lime, Silica Fume and Rice Husk ash. https://doi.org/10.3390/pr10071424.
Malathy, R., Shanmugam, R., Dhamotharan, D., Kamaraj, D., Prabakaran, M., Kim, J., 2023a. Lime based concrete and mortar enhanced with pozzolanic materials – state of art. Constr. Build. Mater. 390, 131415. https://doi.org/10.1016/J.CONBUILDMAT.2023.131415.
Malathy, R., Shanmugam, R., Dhamotharan, D., Kamaraj, D., Prabakaran, M., Kim, J., 2023b. Lime based concrete and mortar enhanced with pozzolanic materials – state of art. Constr. Build. Mater. 390, 131415. https://doi.org/10.1016/J.CONBUILDMAT.2023.131415.
Maravelaki-Kalaitzaki, P., Bakolas, A., Karatasios, I., Kilikoglou, V., 2005. Hydraulic lime mortars for the restoration of historic masonry in Crete. Cement Concr. Res. 35, 1577–1586. https://doi.org/10.1016/J.CEMCONRES.2004.09.001.
Marques, A.I., Morais, J., Morais, P., Veiga, M. do R., Santos, C., Candeias, P., Ferreira, J. G., 2020. Modulus of elasticity of mortars: static and dynamic analyses. Constr. Build. Mater. 232, 117216. https://doi.org/10.1016/J.CONBUILDMAT.2019.117216.
Marques, S.F., Ribeiro, R.A., Silva, L.M., Ferreira, V.M., Labrincha, J.A., 2006. Study of rehabilitation mortars: construction of a knowledge correlation matrix. Cement Concr. Res. 36, 1894–1902. https://doi.org/10.1016/J.CEMCONRES.2006.06.005.
Matos, A.M., Nunes, S., Costa, C., Aguiar, J.L.B., 2021. Durability of an UHPC containing spent equilibrium catalyst. Constr. Build. Mater. 305, 124681. https://doi.org/10.1016/J.CONBUILDMAT.2021.124681.
Matos, A.M., Nunes, S., Costa, C., Barroso-Aguiar, J.L., 2019. Spent equilibrium catalyst as internal curing agent in UHPFRC. Cem. Concr. Compos. 104, 103362. https://doi.org/10.1016/j.cemconcomp.2019.103362.
Mineral Products Association, 2023a. Lime: Net Negative 2040 Roadmap. https://mineralproducts.org/MPA/media/root/Publications/2023/Lime_Net_Negative_2040_Roadmap.pdf.
Montgomery, D.C., 2012. Design and Analysis of Experiments, Eighth. John Wiley & Sons, Inc. https://www.amazon.com/Design-Analysis-Experiments-Douglas-Montgomery/dp/1118146921. (Accessed 19 January 2022).
Mosquera, M.J., Silva, B., Prieto, B., Ruiz-Herrera, E., 2006. Addition of cement to lime-based mortars: Effect on pore structure and vapor transport. Cement Concr. Res. 36 (9), 1635–1642. https://doi.org/10.1016/j.cemconres.2004.10.041.
Nalon, G.H., Alves, M.A., Pedroti, L.G., Lopes Ribeiro, J.C., Hilarino Fernandes, W.E., Silva de Oliveira, D., 2021. Compressive strength, dynamic, and static modulus of cement-lime laying mortars obtained from samples of various geometries. J. Build. Eng. 44, 102626. https://doi.org/10.1016/J.JOBE.2021.102626.
Nunes, S., Matos, A.M., Duarte, T., Figueiras, H., Sousa-Coutinho, J., 2013. Mixture design of self-compacting glass mortar. Cem. Concr. Compos. 43, 1–11. https://doi.org/10.1016/j.cemconcomp.2013.05.009.
Oloruntoba, A., Zhang, Y., Hsu, C.S., 2022. State-of-the-Art review of Fluid Catalytic Cracking (FCC) catalyst regeneration intensification technologies. Energies 15, 2061. https://doi.org/10.3390/EN15062061.
Pavía, S., Walker, R., Veale, P., Wood, A., 2014. Impact of the properties and reactivity of Rice Husk ash on lime mortar properties. J. Mater. Civ. Eng. 26, 04014066. https://doi.org/10.1061/(ASCE)MT.1943-5533.0000967.

Pavía, S., Hanley, R., 2010. Flexural bond strength of natural hydraulic lime mortar and clay brick. Materials and Structures/Materiaux et Constructions 43, 913–922. https://doi.org/10.1617/S11527-009-9555-2/FIGURES/5.

Quarcioni, V.A., Chotoli, F.F., Br, F., V Coelho, A.C., Br, A., Cincotto, M.A., 2015. Indirect and direct Chapelle's methods for the determination of lime consumption in pozzolanic materials. Revista IBRACON de Estruturas e Materiais 8, 1–7. https://doi.org/10.1590/S1983-41952015000100002.

Ramesh, M., Azenha, M., Lourenço, P.B., 2019. Quantification of impact of lime on mechanical behaviour of lime cement blended mortars for bedding joints in masonry systems. Constr. Build. Mater. 229, 116884. https://doi.org/10.1016/J.CONBUILDMAT.2019.116884.

Rattanasak, U., Jaturapitakkul, C., Sudaprasert, T., 2001. Compressive strength and heavy metal leaching behaviour of mortars containing spent catalyst. https://doi.org/10.1177/0734242X0101900511.

Rodrigues, J.D., Grossi, A., 2007. Indicators and ratings for the compatibility assessment of conservation actions. J. Cult. Herit. 8, 32–43. https://doi.org/10.1016/J.CULHER.2006.04.007.

Rosário Veiga, M., Fragata, A., Velosa, A.L., Magalhães, A.C., Margalha, G., 2010. Lime-Based mortars: viability for use as substitution renders in historical buildings. International Journal of Architectural Heritage Conservation, Analysis, and Restoration 4, 177–195. https://doi.org/10.1080/15583050902914678.

Ruiz, G., Aguilar, R., Nakamatsu, J., Kim, S., 2019. Synthesis of a geopolymer binders using spent Fluid Catalytic Cracking (FCC) catalyst. IOP Conf. Ser. Mater. Sci. Eng. 660, 012009. https://doi.org/10.1088/1757-899X/660/1/012009.

Sadeghbeigi, R., 2012. Fluid Catalytic Cracking Handbook: An Expert Guide to the Practical Operation, Design, and Optimization of FCC Units, third ed. Butterworth-Heinemann, Oxford, UK, ISBN 978-0-12-386965-4.

Segura, J., Aponte, D., Pelà, L., Roca, P., 2020. Influence of recycled limestone filler additions on the mechanical behaviour of commercial premixed hydraulic lime based mortars. Constr. Build. Mater. 238, 117722. https://doi.org/10.1016/J.CONBUILDMAT.2019.117722.

Shan, Y., Liu, Z., Guan, D., 2016a. CO2 emissions from China's lime industry. Appl. Energy 166, 245–252. https://doi.org/10.1016/J.APENERGY.2015.04.091.

Su, N., Fang, H.Y., Chen, Z.H., Liu, F.S., 2000. Reuse of waste catalysts from petrochemical industries for cement substitution. Cement Concr. Res. 30, 1773–1783. https://doi.org/10.1016/S0008-8846(00)00401-4.

United Nations, 2015. Transforming our World: the 2030 Agenda for Sustainable Development.

Verified Market Research, 2024b. https://www.verifiedmarketresearch.com/product/lime-mortar-market/. (Accessed 7 February 2025).

Vogt, E.T.C., Weckhuysen, B.M., 2015. Fluid catalytic cracking: recent developments on the grand old lady of zeolite catalysis. Chem. Soc. Rev. 44, 7342–7370. https://doi.org/10.1039/C5CS00376H.

Wang, H., Shang, J., Zhou, L., Gu, Z., Xiao, Wang, R., Solouki, A., Al-Tabbaa, A., Wang, X., Shang, H., Zhou, J., Gu, L., Xiao, Z., Wang, X., Wang, R., 2024. Enhancing hydraulic lime mortar with Metakaolin: a Study on improving restoration materials for historic buildings. Materials 17, 3548. https://doi.org/10.3390/MA17143548.

Zhang, D., Fang, S., Zhang, H., Liu, Z., Zhang, Z., Zhang, S., 2021. Utilization of spent FCC catalyst as fine aggregate in non-sintered brick: alkali activation and environmental risk assessment. Front. Chem. 9, 674271. https://doi.org/10.3389/FCHEM.2021.674271/BIBTEX.

Zhang, R., Liu, T., Zhang, Y., Cai, Z., Yuan, Y., 2020. Preparation of spent fluid catalytic cracking catalyst-metakaolin based geopolymer and its process optimization through response surface method. Constr. Build. Mater. 264, 120727. https://doi.org/10.1016/j.conbuildmat.2020.120727.

Zhao, P., Shen, Y., Duan, H., Zhang, Y., Li, X., Zhu, P., Zhu, W., Liu, G., Pang, B., Cheng, L., 2024. Development and application of artificial hydraulic lime for Chinese architectural heritage restorations. Constr. Build. Mater. 442, 137582. https://doi.org/10.1016/J.CONBUILDMAT.2024.137582.